IEEE Access
Multidisciplinary | Rapid Review | Open Access Journal

Received December 16, 2019, accepted December 31, 2019, date of publication January 7, 2020, date of current version January 16, 2020.

Digital Object Identifier 10.1109/ACCESS.2020.2964572

Multi-Fault Diagnosis of an Aero-Engine Control System Using Joint Sliding Mode Observers

LINFENG GOU, YAWEN SHEN, HUA ZHENG, AND XIANYI ZENG
School of Power and Energy, Northwestern Polytechnical University, Xi'an 710072, China

Corresponding author: Linfeng Gou (goulinfengnwpu07@163.com)

This work was supported in part by the National Science and Technology Major Project under Grant 2017-V-0011-0062, and in part by the Fundamental Research Funds for the Central Universities under Grant 31020190MS702.

ABSTRACT An aero-engine is a complex aerodynamic thermal system, which can operate in extreme environments for long periods. It is crucial to diagnose any faults of the aero-engine control system accurately. At present, most aero-engine control system fault diagnosis schemes suffer from large interference, significant chattering, and low estimation accuracy. To diagnose multi-faults of the control system effectively, we introduce and investigate a new fault diagnosis scheme in this paper, which uses joint sliding mode observers. First, we develop a mathematical model for multi-faults in the control system, which can describe actuator and sensor faults in detail. Then, we design the joint sliding mode observers for fault detection and isolation (FDI), using the sliding mode variable structure term to reduce the coupling effect. Finally, during the fault estimation process, we use a pseudo-sliding form to reduce the chattering problem and suppress the impact of interference, which leads to an accurate estimation of the multi-fault characteristics. The simulation results show that, the proposed scheme can effectively detect and isolate faults, which enables superior timeliness and accuracy compared to a conventional sliding mode observer scheme. During the process of fault estimation, the effect of chattering is reduced, which shows the advantages of strong sensitivity and high estimation accuracy.

INDEX TERMS Aero-engine, control system, fault diagnosis, sliding mode observer.

I. INTRODUCTION

An aero-engine is an aerodynamic thermal system that integrates technologies such as aircraft, electricity, gas, and fluid. Due to the complex aero-engine structure and the harsh operating environments, as the operating time increases, the reliability decreases gradually, and the occurrence of faults is inevitable [1], [2]. To improve the stability and safety of aero-engines, and to extend the service life, it is crucial to diagnose all faults accurately and effectively [3]. In this paper, we use a turbofan engine as research object and analyze the control system faults.

Researchers, worldwide, have proposed plenty of methods that require observers for control system fault diagnosis. At present, the Luenberger observer [4], Kalman filter (KF) [5], and sliding mode observer (SMO) [6], [7] are commonly used. The conventional observer was first proposed by Luenberger, who used linear feedback to estimate the form of the error. Although the Luenberger observer has good fault detection sensitivity, due to uncertainties such as noise, interference, and time-varying parameters of the aero-engine, the Luenberger observer suffers from inaccurate estimate severely [8]. The Kalman filter is robust for systems with white noise but is less robust for systems with white noise but less so for systems where interference does not come in the form of Gaussian white noise [9]. Due to the strong nonlinearity of a turbofan engine, its accuracy is high near the modeling area when linearizing. However, a modeling error occurs throughout the life cycle. When multi-faults occur, there is strong coupling between different faults, which results in a Kalman filter estimation accuracy that cannot meet the requirements [10]. In addition, the extended Kalman Filter (EKF) [11], cubature Kalman filter (CKF) [12] and unscented Kalman filter (UKF) [13] have been improved due to an improved Kalman filter algorithm. However, there are some shortcomings, such as a large initial error and inaccurate estimates for strong nonlinear systems.

The associate editor coordinating the review of this manuscript and approving it for publication was Rosario Pecora.

This work is licensed under a Creative Commons Attribution 4.0 License. For more information, see http://creativecommons.org/licenses/by/4.0/

Sliding mode control (SMC) [14] was first proposed by the Soviet scholar Emelyanov in the 1960s. During the development of the sliding mode observer, Utkin [15] first used discontinuous switching items. Subsequently, Walcott and Zak [16] used a Lyapunov-based method to construct observers with discontinuous terms, and the Thau observer [17] was designed for nonlinear systems. The sliding mode observer feeds the output estimation error back via a nonlinear switching term, which effectively solves the problem that the state estimation cannot approach the system state due to unknown interference [18], and increases robustness. Sliding mode theory has been continuously developed for decades, and the areas of application of this method have been expanding. In recent years, SMO-based fault diagnosis methods were studied extensively [19]. However, the sliding mode observer represents a discontinuous control system. When reaching the sliding surface, the state trajectory traverses back and forth on both sides of the sliding surface, which causes the well-known chattering problem [20]–[22]. In addition, coupling between different faults has an adverse effect on the fault diagnosis results. To make better use of SMO for aero-engine control system fault diagnosis, the following problems need to be solved: 1) Existing control system fault models cannot describe multi-faults accurately; 2) Due to coupling between different faults [23], problems such as insensitive reaction, false positives and false negatives may occur during the fault diagnosis process; 3) The chattering problem of the sliding mode observer affects the estimation accuracy negatively [24].

To make up for the shortcomings of the conventional sliding mode observer, we design a more effective multi-fault diagnosis scheme for the aero-engine control system using joint sliding mode observers, which can describe all possible faults by multi-fault model. During the FDI process, the sliding mode variable structure term can weaken coupling between different faults, and increase the sensitivity of FDI. The proposed scheme also can suppress the impact of uncertain factors for fault estimation. This method shows a strong fault identification and separation capability, and improves the estimation accuracy, which has the following advantages compared to the conventional sliding mode observer method:

1 It represents a more comprehensive multi-fault model for aero-engine control systems, and it supplies a more accurate description of multi-faults, thereby laying the foundation for a fully-fledged multi-fault diagnosis.
2 Design of joint sliding mode observers for FDI: Each of these observers corresponds to a specific fault, which reduces the coupling effect and improves the accuracy of the fault diagnosis.
3 During fault estimation, we use a pseudo-sliding form to reduce the chattering problem and suppress the impact of interference by H_∞ design. This leads to an accurate estimation of the multi-fault characteristics.

The content of other sections in this paper are as follows: In Section. II, a multi-fault model for the control system is presented. The scheme using joint sliding mode observers for multi-fault diagnosis is established in Section. III. In Section. IV, some simulation and verification results are given to evaluate the scheme proposed in this paper. Section. V concludes the results and discusses the future direction of related research.

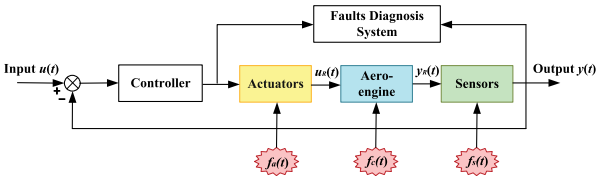

FIGURE 1. Shematic diagram of aero-engine control system fault.

II. FAULT MODEL

The aero-engine control system consists of actuators, a dynamic system, and sensors [25]. In this section, we study the actuator faults and sensor faults, and analyze the typical fault model and mechanism of the actuators and sensors. Then, we establish a mathematical model for multi-faults in an aero-engine control system.

A. TYPICAL FAULT MODEL

Faults may occur in actuators, system components and sensors [26], [27], as shown in Fig. 1, which are denoted by $f_a(t)$, $f_c(t)$ and $f_s(t)$, respectively. In this paper, we study actuator faults and sensor faults diagnosis of the control system.

Because actuator faults can interrupt or change the output value of the controller [28], the controlled object cannot receive the required input [29], and the sensor faults can change the output value, which can produce inaccurate measurement information [30]. Both actuator faults and sensor faults usually do not affect the characteristics of the controlled object [31]. Typical fault modes for actuators and sensors [32] include stuck, constant gain changes, constant deviations, and other abnormal behavior. In the control system, $u_R(t)$ represents the stimulus-response to the control input $u(t)$. If actuator faults occur, $u_R(t)$ can be described as

$$u_R(t) = u(t) + f_a(t). \tag{1}$$

The actual output value is usually not directly available, and the value needs to be measured by sensors [33]. If sensor faults occur, the measurement output value can be described as:

$$y(t) = y_R(t) + f_s(t). \tag{2}$$

B. MULTI-FAULT MODEL

Accounting for control system uncertainties, when multi-faults occur [34], the model can be formulated as:

$$\begin{cases} \dot{x}(t) = Ax(t) + f(x,t) + B(u(t) + f_a(t)) + Ed(t) \\ y(t) = Cx(t) + Df_s(t), \end{cases} \tag{3}$$

where $x \in R^n$, $u \in R^m$, and $y \in R^p$ represent state, input, and output variables respectively. $f_a \in R^m$ represents actuator faults, and $f_s \in R^q$ represents sensor faults. $f(x,t)$ is the bounded nonlinear function, which satisfies the Lipschitz condition. $d \in R^r$ represents bounded system uncertainties. $A \in R^{n\times n}$, $B \in R^{n\times m}$, $C \in R^{p\times q}$, $E \in R^{n\times r}$, are constant matrixes, among which B and D are of full rank, so that when some actuator or sensor faults occur, other parts are still working normally. In other words, the operation of each actuator and sensor is independent, and they have no effect on each other.

The aero-engine control system is complex and changeable. To establish the multi-fault model that satisfies the requirements and implement fault diagnosis more effectively, we make the following assumptions on the related matrixes, the boundedness of the actuator and sensor faults, and the nonlinear part characteristics.

Assumption 1: (A, C) is observable.

Assumption 2: The actuator faults, sensor faults and system uncertainties are bounded functions, i.e. $\|f_{ai}\| \leqslant \lambda_i$, $\|f_{sj}\| \leqslant \lambda_j$, $\|d\| \leqslant \lambda_d$, where λ_i, λ_j, and λ_d are constants greater than 0.

Assumption 3: Nonlinear function $f(x,t)$ conforms to Lipschitz condition for x, i.e. $\forall x, x \in R^n$, there is

$$\left\|f(x,t) - f\left(\hat{x},t\right)\right\| \leqslant L_{f1}\left\|x - \hat{x}\right\|, \tag{4}$$

where L_f represents the Lipschitz constant.

Based on the above assumptions, the following fault model can be formulated for possible fault conditions:

$$\begin{cases} \dot{x}(t) = Ax(t) + f(x,t) + Bu(t) \\ \qquad + \sum_{i=1}^{\alpha} B_{mi} f_{ami}(t) + Ed(t) \\ y(t) = Cx(t) + \sum_{j=1}^{\beta} D_{qj} f_{sqj}(t). \end{cases} \tag{5}$$

When establishing the multi-fault model, the following content about equation (5) need to be stated:

(1) $B = \left[B_1 \cdots B_i \cdots B_m\right]$,where B_i is the i-th column vector of B.

(2) $D = \left[D_1 \cdots D_j \cdots D_q\right]$,where D_j is the j-th column vector of D.

(3) f_{ami} denotes the i-th actuator fault when α ($\alpha \leqslant m$) actuator faults occur simultaneously, while B_{mi} denotes the column vector of the i-th ($i = 1, 2, \cdots, \alpha$) actuator fault.

(4) f_{sqj} denotes the j-th sensor fault when β ($\beta \leqslant q$) sensor faults occur simultaneously, while D_{qj} denotes the column vector of the j-th ($j = 1, 2, \cdots, \beta$) actuator fault.

(5) Possible fault conditions: $\alpha(\alpha \leqslant m)$ actuator faults and $\beta(\beta \leqslant q)$ sensor faults can occur simultaneously.

The integral observer can efficiently estimate unknown inputs. Therefore, for sensor faults, we use the integral observer (6) and (7) to transform them into pseudo-actuator faults, consequently, a control system multi-fault model can be established to accurately describe the actuator and sensor faults. Other than that, actuator and sensor faults are expressed in the same form, so the same method can be used to diagnose actuator and sensor faults, which simplifies the design of the fault diagnosis scheme.

$$\varphi = \int_0^t y(\tau)\, d\tau, \tag{6}$$

i.e.

$$\dot{\varphi} = Cx(t) + \sum_{j=1}^{\beta} D_{qj} f_{sqj}(t). \tag{7}$$

A new control system equation can be obtained using (5) and (7):

$$\begin{cases} \begin{bmatrix} \dot{x} \\ \dot{\varphi} \end{bmatrix} = \begin{bmatrix} A & 0 \\ C & 0 \end{bmatrix} \begin{bmatrix} x \\ \varphi \end{bmatrix} + \begin{bmatrix} f(x,t) \\ 0 \end{bmatrix} \\ \qquad + \begin{bmatrix} B \\ 0 \end{bmatrix} u + \sum_{i=1}^{\alpha} \begin{bmatrix} B_{mi} \\ 0 \end{bmatrix} f_{ami}(t) \\ \qquad + \begin{bmatrix} E \\ 0 \end{bmatrix} d + \sum_{j=1}^{\beta} \begin{bmatrix} 0 \\ D_{qj} \end{bmatrix} f_{sqj}(t) \\ \varphi = \begin{bmatrix} 0 & I \end{bmatrix} \begin{bmatrix} x \\ \varphi \end{bmatrix}. \end{cases} \tag{8}$$

By defining $\bar{x} = \begin{bmatrix} x \\ \varphi \end{bmatrix}$, $\bar{y} = \varphi$, substituted into (8) gives:

$$\begin{cases} \dot{\bar{x}}(t) = \bar{A}\bar{x}(t) + \bar{f}(x,t) \\ \qquad + \bar{B}u(t) + \sum_{i=1}^{\alpha} \bar{B}_{mi} f_{ami}(t) \\ \qquad + \bar{E}d(t) + \sum_{j=1}^{\beta} \bar{D}_{qj} f_{sqj}(t) \\ \bar{y}(t) = \bar{C}\bar{x}(t) \end{cases} \tag{9}$$

The matrix parameters in (9) are

$$\begin{aligned} &\bar{A} = \begin{bmatrix} A & 0 \\ C & 0 \end{bmatrix}, \quad \bar{f}(x,t) = \begin{bmatrix} f(x,t) \\ 0 \end{bmatrix}, \\ &\bar{B} = \begin{bmatrix} B \\ 0 \end{bmatrix}, \quad \bar{B}_{mi} = \begin{bmatrix} B_{mi} \\ 0 \end{bmatrix}, \\ &\bar{E} = \begin{bmatrix} E \\ 0 \end{bmatrix}, \quad \bar{C} = \begin{bmatrix} 0 & I \end{bmatrix}, \\ &\bar{D} = \begin{bmatrix} 0 \\ D \end{bmatrix}, \quad \bar{D}_{qj} = \begin{bmatrix} 0 \\ D_{qj} \end{bmatrix}. \end{aligned} \tag{10}$$

Equation (9) means that both sensor and actuator faults have the same form. This can be further organized into

$$\begin{cases} \dot{\bar{x}}(t) = \bar{A}\bar{x}(t) + \bar{f}(x,t) + \bar{B}u(t) \\ \qquad + \sum_{k=1}^{\alpha+\beta} \bar{X}_{(m+q)k} f_k(t) + \bar{E}d(t), \\ \bar{y}(t) = \bar{C}\bar{x}(t) \end{cases} \tag{11}$$

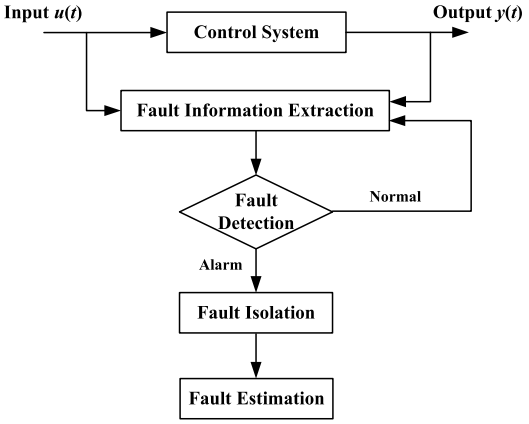

FIGURE 2. Structure diagram of control system fault diagnosis.

where $\sum_{k=1}^{\alpha+\beta} \bar{X}_{(m+q)k} f_k(t)$ is the general term for $\sum_{i=1}^{\alpha} \bar{B}_{mi} f_{ami}(t)$ and $\sum_{j=1}^{\beta} \bar{G}_{qj} f_{sqj}(t)$, and all types of control system faults are uniformly denoted by f. $\alpha+\beta$, $(\alpha+\beta \leqslant m+q)$ represents the total number of possible faults. $f_k(t)$ represents the k-th $(k = 1, 2, \cdots, \alpha+\beta)$ fault, and $\bar{X}_{(m+q)k}$ represents the column vector of $\bar{X}$. The relationship of the full rank matrix $\bar{X}$, $\bar{B}$ and $\bar{D}$ can be expressed as

$$\bar{X} = \begin{bmatrix} \bar{B} & \bar{D} \end{bmatrix}. \tag{12}$$

Equation (11) can also be expressed as

$$\begin{cases} \dot{\bar{x}}(t) = \bar{A}\bar{x}(t) + \bar{f}(x,t) + \bar{B}u(t) + \bar{X}f(t) + \bar{E}d(t) \\ \bar{y}(t) = \bar{C}\bar{x}(t). \end{cases} \tag{13}$$

In the above process, we transform sensor faults into pseudo-actuator faults through the introduction of the integral observer φ, which simplifies the design of fault diagnosis scheme, while it still fully describes the system faults.

III. MULTI-FAULT DIAGNOSIS SCHEME

In this section, we use joint sliding mode observers to establish the multi-fault diagnosis scheme. Firstly, we design observers for the multi-fault model in Section. II to realize FDI. The second step is to design observers for fault estimation. The effect of the uncertainties on the system is attenuated to a minimum level by the H_∞ design [35], [36], which means the fault characteristics can be estimated accurately. Fig. 2 shows the fault diagnosis structure diagram.

A. FDI SCHEME

In this paper, we design observers for various types of faults to construct the joint sliding mode observers. In order to promote the application to nonlinear systems with sensor and actuator faults and ensure the accuracy of the proposed scheme, before designing the observers, we make the following assumptions:

Assumption 4: $(\bar{A}, \bar{C})$ is observable. There exists a matrix L, which makes $\bar{A}_0 = \bar{A} - L\bar{C}$ stable matrix.

Assumption 5: The nonlinear function $\bar{f}(x,t)$ conforms to the Lipschitz condition for x, i.e. $\forall x, x \in R^n$, and there is

$$\left\| \bar{f}(x,t) - \bar{f}(\hat{x},t) \right\| \leqslant L_{f2} \left\| x - \hat{x} \right\|, \tag{14}$$

where L_{f2} is Lipschitz constant.

Assumption 6: There exist matrixes P and F, which satisfy $P\bar{X}_{(m+q)k} = \bar{C}^T F^T$, where P is a real symmetric positive definite matrix.

Assumption 7: Q is a real symmetric positive definite matrix, which satisfies the Lyapunov equation $A_0^T P + PA_0 = -Q$.

When the control system faults occur, the SMO designed for the l-th $(l = 1, 2, \cdots, \alpha+\beta)$ fault in system (11), based on the above assumptions, is:

$$\begin{cases} \dot{\hat{\bar{x}}}_l = \bar{A}\hat{\bar{x}} + \bar{f}(\hat{x},t) + \bar{B}u + L\left(\bar{y} - \hat{\bar{y}}\right) + \sum_{k=1,k\neq l}^{\alpha+\beta} \bar{X}_{(m+q)k} v_k \\ \hat{\bar{y}} = \bar{C}\hat{\bar{x}}, \end{cases} \tag{15}$$

where $\hat{\bar{x}}$ and $\hat{\bar{y}}$ represent the estimated values of $\bar{x}$ and $\bar{y}$ respectively. v_k is the sliding mode variable structure term, which can cut off the impact of the remaining faults $f_{(\alpha+\beta)k}(k = 1, 2 \ldots\ldots \alpha+\beta, k \neq l)$ on the system, and L is the gain matrix. When the l-th $(l = 1, 2, \cdots, \alpha+\beta)$ fault occurs. v_k is expressed as

$$v_k = \begin{cases} \rho_k \dfrac{F_{(m+q)k}\left(\bar{y} - \hat{\bar{y}}\right)_k}{\left\| F_{(m+q)k}\left(\bar{y} - \hat{\bar{y}}\right)_k \right\|} & , \left(\bar{y} - \hat{\bar{y}}\right)_k \neq 0 \\ 0 & , \left(\bar{y} - \hat{\bar{y}}\right)_k = 0, \end{cases} \tag{16}$$

where ρ_k is the sliding mode variable structure parameter [37], $\rho_k > 0$. $\left(\bar{y} - \hat{\bar{y}}\right)_k$ is the k-th $(k = 1, 2, \cdots, a+b, k \neq l)$ column vector of $\bar{y} - \hat{\bar{y}}$, and $F_{(m+q)k}$ is the k-th row vector of the matrix F.

When multi-faults occur in the control system, we need to design joint sliding mode observers. Each observer is directed to a specific type of fault, which means that residuals for all faults can be generated. Then, we can determine whether faults have occurred and the specific parts of faults based on the residuals. We now define the state estimation error $\bar{e} = \bar{x} - \hat{\bar{x}}$ and the measurement error $\bar{e}_y = \bar{y} - \hat{\bar{y}}$. When multi-faults occur in the aero-engine control system, the state estimation error that corresponds to the l-th fault can be expressed as

$$\begin{aligned} \dot{\bar{e}}_l &= \dot{\bar{x}} - \dot{\hat{\bar{x}}}_l \\ &= \bar{A}\bar{x} + \bar{f}(x,t) + \bar{B}u + \sum_{k=1}^{\alpha+\beta} \bar{X}_{(m+q)k} f_{(m+q)k} + \bar{E}d \\ &\quad - \bar{A}\hat{\bar{x}} - \bar{f}(\hat{x},t) - \bar{B}u - L\left(\bar{y} - \hat{\bar{y}}\right) - \sum_{k=1,k\neq l}^{\alpha+\beta} \bar{X}_{(m+q)k} v_k \\ &= \left(\bar{A} - L\bar{C}\right)\bar{e}_l + \bar{f}(x,t) - \bar{f}(\hat{x},t) \\ &\quad + \sum_{k=1,k\neq l}^{\alpha+\beta} \bar{X}_{(m+q)k}(f_k - v_k) + \bar{X}_{(m+q)l} f_l + \bar{E}d. \end{aligned} \tag{17}$$

Based on the previous assumptions, we select the Lyapunov function [38]

$$V = \bar{e}^T P \bar{e}. \tag{18}$$

(1) Assuming that, when multi-faults occur, not including the g-th fault, we can obtain

$$\dot{\bar{e}}_g = \left(\bar{A} - L\bar{C}\right)\bar{e}_g + \bar{f}\left(x,t\right) - \bar{f}\left(\hat{x},t\right) + \sum_{k=1,k\neq g}^{\alpha+\beta} \bar{X}_{(m+q)g}(f_k - v_k) + \bar{E}d. \tag{19}$$

The derivation of the Lyapunov function [39], [40] is:

$$\begin{aligned}\dot{V} &= \bar{e}_g^T\left(-Q\right)\bar{e}_g + 2\bar{e}_g^T P\left(\bar{f}\left(x,t\right) - \bar{f}\left(\hat{x},t\right)\right) \\ &\quad + 2\bar{e}_g^T P\bar{E}d + 2\bar{e}_g^T P\sum_{k=1,k\neq g}^{\alpha+\beta}\bar{X}_{(m+q)g}(f_k - v_k) \\ &\leqslant \bar{e}_g^T\left(-Q\right)\bar{e}_g + L_{f2}^2\left\|\bar{e}_g P\right\|^2 + \left\|\bar{e}_g\right\|^2 + 2\left\|\bar{E}\right\|\left\|P\bar{e}_g\right\|\lambda_d \\ &\quad - 2\bar{e}_g^T\left(\sum_{k=1,k\neq g}^{\alpha+\beta}\left\|F_{(m+q)k}\left(\bar{y}-\hat{\bar{y}}\right)_k\right\|\left(\rho_k - \max\left\{\lambda_i,\lambda_j\right\}\right)\right) \\ &\leqslant \bar{e}_g^T\left(-Q + L_{f2}^2 PP + I + 2\bar{E}P\lambda_d\right)\bar{e}_g. \end{aligned} \tag{20}$$

When satisfying $\begin{bmatrix} -Q + I + 2\bar{E}P\lambda_d & P \\ P & -\frac{1}{L_{f2}^2} \end{bmatrix} < 0$ and $\rho_k > \max\left\{\lambda_i,\lambda_j\right\}$, we can get $\dot{V} < 0$, so that $\lim_{t\to\infty}\bar{e}_g = 0$.

(2) Assuming that, when multi-faults occur, including the z-th fault, we can get

$$\dot{\bar{e}}_z = \left(\bar{A} - L\bar{C}\right)\bar{e}_z + \bar{f}\left(x,t\right) - \bar{f}\left(\hat{x},t\right) + \sum_{k=1,k\neq z}^{\alpha+\beta}\bar{X}_{(m+q)k}(f_k - v_k) + \bar{X}_{(m+q)z}f_z + \bar{E}d, \tag{21}$$

Because the matrix $\bar{X}$ is full rank, so that $\bar{X}_{(m+q)k}$ is independent of $\bar{X}_{(m+q)z}$ linearity, $\lim_{t\to\infty}\bar{e}_z \neq 0$.

We can determine that, when $k(k \leqslant \alpha+\beta)$ faults occur in the control system, k corresponding state estimation errors $\bar{e}_{(k)}$ cannot converge to the zero domain, and the remaining $\alpha+\beta-k$ state estimation errors $\bar{e}_{(\alpha+\beta-k)}$ can quickly converge to the zero domain.

When the l-th $(l = 1,2,\cdots,\alpha+\beta)$ fault in the control system occurs, the corresponding residual is as follows:

$$r_l = \left\|\bar{e}_{yl}\right\|. \tag{22}$$

When k faults occur simultaneously, the corresponding residuals are

$$r_{(k)} = \left\|\bar{e}_{y(k)}\right\|. \tag{23}$$

This time, the residual of the overall system is

$$r = \sum_{k=1}^{\alpha+\beta}\left\|\bar{e}_{yk}\right\|. \tag{24}$$

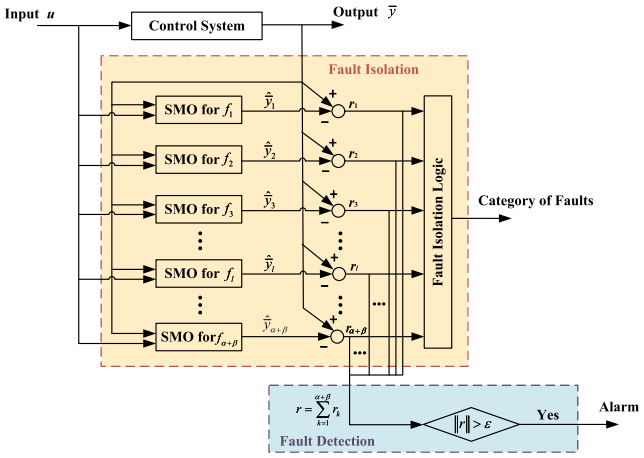

FIGURE 3. Multi-fault detection and isolation scheme.

Based on the above analysis, the FDI scheme using the joint sliding mode observers in this paper, is as shown in Fig. 3. The scheme can be described as: When faults occur, the overall system residual does not converge to the zero domain. Then we can detect the occurrence of faults in this way. When k $(k \leqslant \alpha+\beta)$ faults occur simultaneously, their corresponding residuals $r_{(k)}$ are sensitive to the faults and do not converge to the zero domain $\varepsilon_{(k)}$, while the remaining $\alpha+\beta-k$ residuals $r_{(\alpha+\beta-k)}$ are insensitive to the faults and converge to the corresponding zero domains $\varepsilon_{(\alpha+\beta-k)}$. Therefore, fault isolation can be performed using the relationship between the residual magnitude and the zero domain. The FDI decision logic is shown in TABLE 1.

B. FAULT ESTIMATION SCHEME

After the faults were accurately isolated, we design the observers to estimate the fault characteristics. When multi-faults occur in the control system, we need to design an observer for each specific fault to estimate the characteristics. In this section, we use the l-th fault f_l as an example to design the SMO:

$$\begin{cases}\dot{\hat{\bar{x}}}_l = \bar{A}\hat{\bar{x}} + \bar{f}\left(\hat{x},t\right) + \bar{B}u - L\left(\bar{y} - \hat{\bar{y}}\right) + v'_l \\ \hat{\bar{y}} = \bar{C}\hat{\bar{x}}. \end{cases} \tag{25}$$

The sliding mode variable structure term v'_l can eliminate the effect of uncertainties, so that the residual contains only fault information [41], which can be expressed as follows:

$$v'_l = \begin{cases} \rho'_l\dfrac{F_{(m+q)l}\left(\bar{y}-\hat{\bar{y}}\right)_l}{\left\|F_{(m+q)r}\left(\bar{y}-\hat{\bar{y}}\right)_l\right\|}, & \left(\bar{y}-\hat{\bar{y}}\right)_l \neq 0 \\ 0, & \left(\bar{y}-\hat{\bar{y}}\right)_l = 0, \end{cases} \tag{26}$$

where the sliding mode variable structure parameter $\rho'_l > 0$.

We define the state estimation error $\bar{e}' = \bar{x} - \hat{\bar{x}}$ and the measurement error $\bar{e}'_y = \bar{y} - \hat{\bar{y}}$. When multi-faults occur, we can use $\bar{e}'$ to estimate the fault f_l, which can be expressed

TABLE 1. FDI Decision Logic.

Residual / Fault	r_1 / f_{am1}	r_2 / f_{am2}	$\cdots$	r_α / $f_{am\alpha}$	$r_{\alpha+1}$ / f_{sq1}	$r_{\alpha+2}$ / f_{sq2}	$\cdots$	$r_{\alpha+\beta}$ / $f_{sq\beta}$	FDI Decision Logic
Residuals	0	0	$\cdots$	0	0	0	$\cdots$	0	fault-free
	1	0	$\cdots$	0	0	0	$\cdots$	0	only f_{am1}
	$\vdots$	$\vdots$	$\vdots$	$\vdots$	$\vdots$	$\vdots$	$\vdots$	$\vdots$	$\vdots$
	1	1	$\cdots$	0	0	0	$\cdots$	0	f_{am1} to $f_{am(\alpha-1)}$
	1	1	$\cdots$	0	0	0	$\cdots$	0	all f_a
	1	1	$\cdots$	1	0	0	$\cdots$	0	all f_a and f_{sq1}
	$\vdots$	$\vdots$	$\vdots$	$\vdots$	$\vdots$	$\vdots$	$\vdots$	$\vdots$	$\vdots$
	1	1	$\cdots$	1	1	1	$\cdots$	0	only $f_{sq\beta}$ free
	1	1	$\cdots$	1	1	1	$\cdots$	1	all faults
	0	1	$\cdots$	1	1	1	$\cdots$	1	only f_{am1} free
	$\vdots$	$\vdots$	$\vdots$	$\vdots$	$\vdots$	$\vdots$	$\vdots$	$\vdots$	$\vdots$
	0	0	$\cdots$	1	1	1	$\cdots$	1	all f_s and $f_{am\alpha}$
	0	0	$\cdots$	0	1	1	$\cdots$	1	all f_s
	0	0	$\cdots$	0	0	1	$\cdots$	1	f_{sq2} to $f_{sq\beta}$
	$\vdots$	$\vdots$	$\vdots$	$\vdots$	$\vdots$	$\vdots$	$\vdots$	$\vdots$	$\vdots$
	0	0	$\cdots$	0	0	0	$\cdots$	1	only $f_{sq\beta}$

as

$$\begin{aligned}\dot{\bar{e}}_l' &= \dot{\bar{x}}_l - \dot{\hat{\bar{x}}}_l \\ &= \bar{A}\bar{x} + \bar{f}(x,t) + \bar{B}u + \bar{X}_{(m+q)l} f_l + \bar{E}d \\ &\quad - \bar{A}\hat{\bar{x}} - \bar{f}(\hat{x},t) - \bar{B}u - L\left(\bar{y} - \hat{\bar{y}}\right) - v'_l \\ &= \left(\bar{A} - L\bar{C}\right)\bar{e}_l + \bar{f}(x,t) - \bar{f}(\hat{x},t) \\ &\quad + \bar{X}_{(m+q)l} f_l - v'_l + \bar{E}d. \end{aligned} \tag{27}$$

After select the Lyapunov function

$$V' = \bar{e}_l'^T P \bar{e}'. \tag{28}$$

And substituting (27) into (28) we obtain:

$$\begin{aligned}\dot{V}' &= \bar{e}_l'^T(-Q)\bar{e}_l' + 2\bar{e}_l'^T P\left(\bar{f}(x,t) - \bar{f}(\hat{x},t)\right) \\ &\quad + 2\bar{e}_l'^T P \bar{X}_{(m+q)l} f_l - 2\bar{e}_l'^T P v_l' \\ &\leqslant \bar{e}_l'^T(-Q)\bar{e}_l' + L_{f2}^2 \left\|\bar{e}_l' P\right\|^2 + \left\|\bar{e}_l'\right\|^2 + 2\rho_l' \left\|P\bar{e}_l'\right\| \\ &\leqslant \bar{e}_l'^T\left(-Q + L_{f2}^2 PP + I + 2P\rho'_r\right)\bar{e}_l'. \end{aligned} \tag{29}$$

When satisfying $\begin{bmatrix} -Q + I + 2P\rho'_r & P \\ P & -\frac{1}{L_{f2}^2} \end{bmatrix} < 0$, we can get $\dot{V}' < 0$, so that $\lim_{t\to\infty} \bar{e}_l' = 0$. The state estimation error is increasingly stable.

Then we select the sliding surface:

$$s = \left\{\left(\bar{e}_l', \bar{e}_{yl}'\right) | \bar{e}_l' = 0\right\}. \tag{30}$$

By adjusting the sliding mode variable structure item, as shown in Fig. 4, $\bar{e}_l'$ can move to the sliding surface in a finite time [42], and then maintain the sliding mode after a certain chattering process [43] to ensure the robustness of the system.

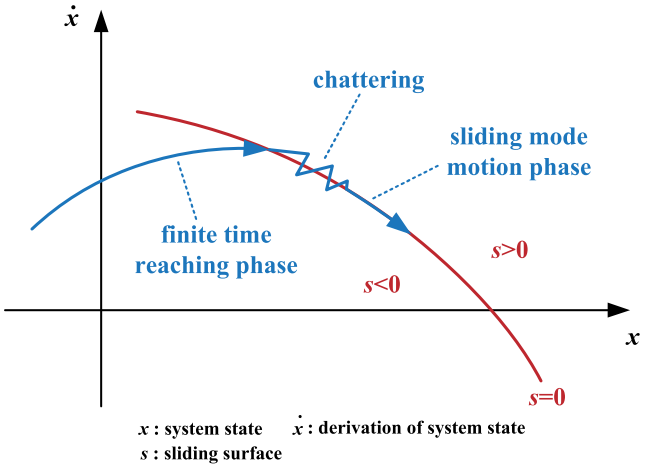

FIGURE 4. Diagram of sliding mode motion.

The existence of uncertainties affects the state estimation error $\bar{e}'$. Therefore, we design H_∞ to suppress the impact of uncertain factors on the residual:

$$\|H\|_\infty = \sup_{||d||_2 \neq 0} \frac{||\bar{e}'||_2}{||d||_2} \leqslant \sqrt{\mu}, \tag{31}$$

where $\mu > 0$, and $||\bullet||_2$ represents a 2-norm.

After the system reaches the sliding surface, it produces ideal sliding motion for a limited time. Then $\dot{\bar{e}}_l' = 0$, $\bar{e}_l' = 0$, and (27) can be written as

$$0 = \left(\bar{A} - L\bar{C}\right)\bar{e}_l + \bar{f}(x,t) - \bar{f}(\hat{x},t) + \bar{X}_{(m+q)l} f_l - v_{eq} + \bar{E}d, \tag{32}$$

where v_{eq} is the equivalent output-error injection, which is required to maintain the sliding mode motion.

To reduce chattering during sliding mode motion, the sliding mode variable structure is usually in the form of pseudo-sliding:

$$v_l' \approx \rho_l' \frac{F_{(m+q)l}\left(\bar{y}-\hat{\bar{y}}\right)_l}{\left\|F_{(m+q)l}\left(\bar{y}-\hat{\bar{y}}\right)_l\right\|+\delta_l}, \tag{33}$$

where δ_l is a positive scalar with a small absolute value to reduce the effect of chattering on the estimation result.

Using the concept of equivalent output-error injection, the fault estimation is expressed as

$$\hat{f}_l = \bar{X}^+_{(m+q)l} v_{eq}, \tag{34}$$

where $\bar{X}^+_{(m+q)l}$ is the pseudo inverse matrix of $\bar{X}_{(m+q)l}$.

Equation (32) can be rewritten as

$$\hat{f}_l - f_l = \bar{X}^+_{(m+q)l}\left(\left(\bar{A}-L\bar{C}\right)\bar{e}_l + \bar{f}\left(x,t\right) - \bar{f}\left(\hat{x},t\right) + \bar{E}d\right). \tag{35}$$

Calculating the 2-norm of (35) yields:

$$\begin{aligned}
&\left\|\hat{f}_l - f_l\right\|_2 \\
&= \left\|\bar{X}^+_{(m+q)l}\left(\left(\bar{A}-L\bar{C}\right)\bar{e}_l + \bar{f}\left(x,t\right) - \bar{f}\left(\hat{x},t\right) + \bar{E}d\right)\right\|_2 \\
&\leqslant \sigma_{\max}\left(\bar{X}^+_{(m+q)l}\left(\bar{A}-L\bar{C}\right)\right)\|\bar{e}_l\|_2 \\
&\quad + \sigma_{\max}\left(\bar{X}^+_{(m+q)l}\right) L_{f2}\|\bar{e}_l\|_2 + \sigma_{\max}\left(\bar{X}^+_{(m+q)l}\bar{E}\right)\|d\|_2 \\
&\leqslant \sigma_{\max}\left(\bar{X}^+_{(m+q)l}\left(\bar{A}-L\bar{C}\right)\right)\|\bar{e}\|_2 \\
&\quad + \sigma_{\max}\left(\bar{X}^+_{(m+q)l}\right) L_{f2}\|\bar{e}\|_2 + \sigma_{\max}\left(\bar{X}^+_{(m+q)l}\bar{E}\right)\|d\|_2.
\end{aligned} \tag{36}$$

Based on the design goal of H_∞, $\|\bar{e}\|_2 \leqslant \sqrt{\mu}\|d\|_2$, the above equation can be rewritten as

$$\begin{aligned}
&\left\|\hat{f}_l - f_l\right\|_2 \\
&\leqslant \sqrt{\mu}\sigma_{\max}\left(\bar{X}^+_{(m+q)l}\left(\bar{A}-L\bar{C}\right)\right)||d||_2 \\
&\quad + \sqrt{\mu}\sigma_{\max}\left(\bar{X}^+_{(m+q)l}\right) L_{f2}||d||_2 + \sigma_{\max}\left(\bar{X}^+_{(m+q)l}\bar{E}\right)\|d\|_2.
\end{aligned} \tag{37}$$

According to the above equation, the error of the fault estimation is related to the system uncertainties. The existence of system uncertainties d affects the accuracy of the fault estimation. Therefore, it is necessary to design a sufficiently small μ to make the SMO retain the fault information effectively.

In summary, when the fault estimation error is within the allowable range, the l-th fault estimation can be approximated using

$$\hat{f}_l = \rho_l' \frac{F_{(m+q)l}\bar{X}^+_{(m+q)l}\left(\bar{y}-\hat{\bar{y}}\right)_l}{\left\|F_{(m+q)l}\left(\bar{y}-\hat{\bar{y}}\right)_l\right\|+\delta_l}. \tag{38}$$

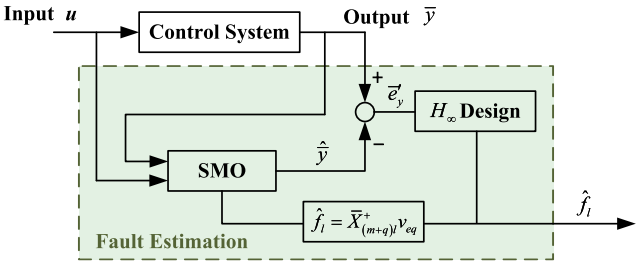

FIGURE 5. Multi-fault estimation scheme.

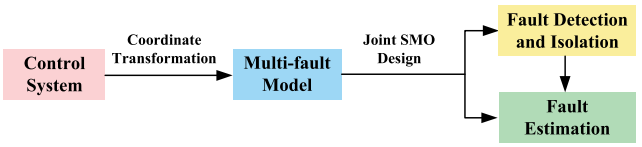

FIGURE 6. Process of the multi-fault diagnosis.

Base on the above analysis, the multi-fault estimation scheme is shown in Fig. 5. When multi-faults occur, we design observers for specific faults, and the term v_l' is used to suppress the interference and uncertainties of the system. At the same time, we can achieve accurate fault estimation through the design of H_∞ and the equivalent output error injection term.

IV. SIMULATION AND VERIFICATION

The multi-fault diagnosis scheme proposed in this paper is mainly divided into three steps. As shown in Fig. 6, the first step is to establish a mathematical model of the aero-engine control system multi-faults. The second step is FDI based on the joint sliding mode observers. The third step is to design a fault estimation scheme after isolating the faults to enable the accurate estimation of multi-faults. The simulation and verification consist of two parts: FDI verification and fault estimation verification.

We verify the scheme using MATLAB/Simulink, taking a twin-shaft turbofan engine as the research object. We select the operating point $H = 7km$, $Ma = 0.6$, $n_f = 2000RPM$.The main parameters are:

$$A = \begin{bmatrix} 0 & 1.0022 & 0 & 0 \\ -47.6554 & -1.2587 & 47.6554 & 0 \\ 0 & 0 & 0 & 10.0128 \\ 1.8521 & 0 & -1.8521 & 0 \end{bmatrix},$$

$$B = \begin{bmatrix} 0 \\ 20.6562 \\ 0 \\ 0 \end{bmatrix}, \quad C = \begin{bmatrix} 0 & 1 & 0 & 0 \\ 0 & 0 & 1 & 0 \\ 0 & 0 & 0 & 1 \end{bmatrix},$$

$$D = \begin{bmatrix} 1 & 0 & 0 \\ 0 & 1 & 0 \\ 0 & 0 & 1 \end{bmatrix}, \quad E = \begin{bmatrix} 1 \\ 0 \\ 1 \\ 1 \end{bmatrix}.$$

$$f\left(x,t\right) = \sin\left(x_3\right), \quad d\left(t\right) = \sin\left(t\right). \tag{39}$$

The following matrixes are obtained via coordinate transformation:

$$\bar{A} = \begin{bmatrix} 0 & 1.0022 & 0 & 0 & 0 & 0 & 0 \\ -47.6554 & -1.2587 & 47.6554 & 0 & 0 & 0 & 0 \\ 0 & 0 & 0 & 10.0128 & 0 & 0 & 0 \\ 1.8521 & 0 & -1.8521 & 0 & 0 & 0 & 0 \\ 1 & 0 & 0 & 0 & 0 & 0 & 0 \\ 0 & 1 & 0 & 0 & 0 & 0 & 0 \\ 0 & 0 & 1 & 0 & 0 & 0 & 0 \end{bmatrix}$$

$$\bar{B} = \begin{bmatrix} 0 \\ 20.6562 \\ 0 \\ 0 \\ 0 \\ 0 \\ 0 \end{bmatrix} \bar{C} = \begin{bmatrix} 0 & 0 & 0 & 0 & 1 & 0 & 0 \\ 0 & 0 & 0 & 0 & 0 & 1 & 0 \\ 0 & 0 & 0 & 0 & 0 & 0 & 1 \end{bmatrix} \bar{E} = \begin{bmatrix} 1 \\ 0 \\ 1 \\ 1 \\ 0 \\ 0 \\ 0 \end{bmatrix}$$

$$\bar{f}(x,t) = \begin{bmatrix} \sin(x_3) \\ 0 \\ 0 \\ 0 \\ 0 \\ 0 \\ 0 \end{bmatrix} \bar{X} = \begin{bmatrix} 0 & 0 & 0 & 0 \\ 20.6562 & 0 & 0 & 0 \\ 0 & 0 & 0 & 0 \\ 0 & 0 & 0 & 0 \\ 0 & 1 & 0 & 0 \\ 0 & 0 & 1 & 0 \\ 0 & 0 & 0 & 1 \end{bmatrix} \tag{40}$$

We now consider the following multi-fault situation:

1) f_{a1}: During $t = 8s \sim 18s$, the jumping fault of a fuel metering valve occurs, whose amplitude is 0.1. At $t = 18s$, the fault disappears. The respective expression is

$$f_{a1} = \begin{cases} 0, & t \leqslant 8s \\ 0.1, & 8s < t < 18s \\ 0, & t \geqslant 18s. \end{cases} \tag{41}$$

2) f_{a2}: During $t = 15s \sim 25s$, the gradual fault of the fuel metering valve occurs, increasing of the slope by $0.03/s$. When $t \geq 25s$, the fault magnitude is maintained at 0.3. The respective expression is

$$f_{a2} = \begin{cases} 0, & t \leqslant 15s \\ 0.03(t-15), & 10s < t < 20s \\ 0.3, & t \geq 25s. \end{cases} \tag{42}$$

3) f_{s1}: During $t = 10s \sim 20s$, the gradual fault of the fan-speed sensor occurs, increasing of the slope by $0.01/s$. When $t \geqslant 20s$, the fault magnitude is maintained at 0.1. The respective expression is

$$f_{s1} = \begin{cases} 0, & t \leqslant 10s \\ 0.01\,(t-10)\,, & 10s < t < 20s \\ 0.1, & t \geqslant 20s. \end{cases} \tag{43}$$

4) f_{s2}: During $t = 20s \sim 30s$, due to external interference, a turbine outlet-temperature sensor sinusoidal fault occurs, whose amplitude is 0.3. The angular frequency is 1 rad/s.

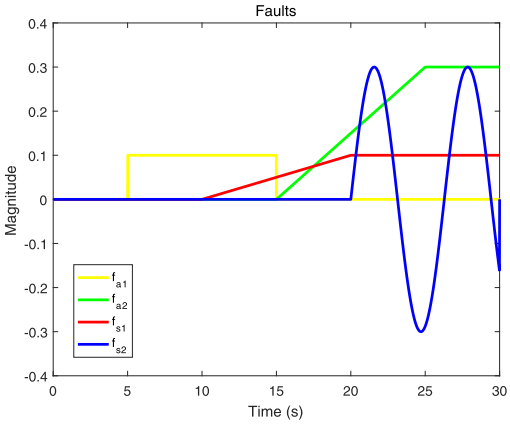

FIGURE 7. Fault information.

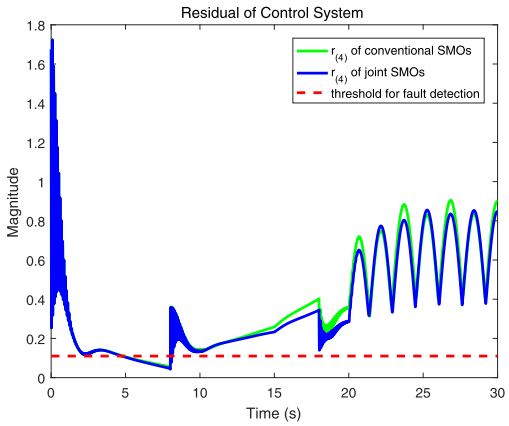

FIGURE 8. Residuals of control system.

At $t = 30s$, the fault disappears. The respective expression is

$$f_{s2} = \begin{cases} 0, & t \leqslant 20s \\ 0.3\sin(t-20)\,, & 20s < t < 30s \\ 0, & t \geqslant 30s \end{cases} \tag{44}$$

We select the following matrixes to satisfy ***assumption 4*** and ***assumption 6***:

$$L = \begin{bmatrix} 1.2387 & 0.2767 & 0.1766 & 0.6878 \\ 0.8165 & -0.0431 & -0.3498 & 0.4377 \\ 0.2533 & 1.5446 & -0.3483 & 1.2546 \\ 0.1298 & -0.1087 & 1.1934 & -0.2458 \\ 2.9879 & -0.0512 & 0.0277 & -0.3901 \\ -0.0295 & 3.0948 & 0.0306 & 1.0548 \\ -0.0249 & 0.0306 & 3.0108 & 0.0476 \end{bmatrix},$$

$$F = \begin{bmatrix} 1.7475 & -0.1873 & -0.0435 \\ -0.1470 & 1.8578 & 0.0629 \\ -0.0583 & 0.0908 & 1.8798 \\ -0.0332 & 1.4377 & 0.2843 \end{bmatrix}. \tag{45}$$

First, we verify the proposed FDI scheme. In the verification process, we compare the joint sliding mode observers with conventional thau observers, and verify the overall system and the above four fault-conditions. The results are shown below:

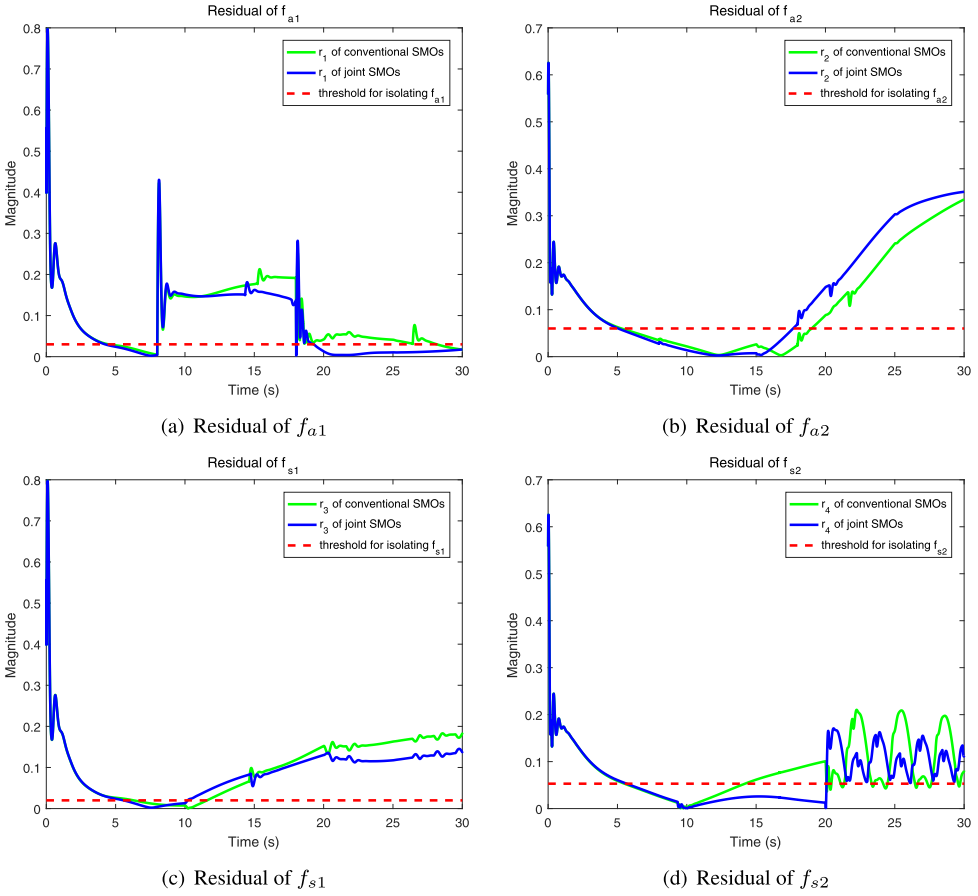

(a) Residual of f_{a1} (b) Residual of f_{a2}

(c) Residual of f_{s1} (d) Residual of f_{s2}

FIGURE 9. Residuals of multi-faults.

The figures show that, during $t = 0s \sim 2s$, because the actual value is different from the estimated value, there are short-term fluctuations of the residuals, which can be ignored during the fault analysis. As can be seen from Fig. 8, in terms of the timeliness of the fault detection, both the conventional method and the proposed method detect faults at about $t = 8s$. For the overall system, the observed results of the two methods are close and both show good timeliness.

In the process of isolating different faults, the defects of the conventional method gradually appear due to coupling between different faults. As shown in Fig. 9, when isolating the fault f_{a1}, it converged to zero during $18s \leqslant t \leqslant 30s$, and the proposed method shows high accuracy. The conventional method, however, still shows the fault occurring within this period of time due to coupling with other faults, which means that a false positive alarm is triggered. When isolating the faults f_{a2} and f_{s1}, because of the positive effect of the sliding mode variable structure term, the joint sliding mode observers can detect and isolate faults more quickly and with better timeliness than the conventional method. When isolating the fault f_{s2}, due to the coupling with other faults, the conventional method shows false alarms during $14s \leqslant t \leqslant 20s$, which reflects lower accuracy. In addition, during several short time-intervals after $t = 20s$, when fault f_{s2} occurs, the conventional method shows that the residual converges to the zero domain, i.e., a false negative alarm is triggered.

After successfully isolating the four faults above, the next step is to estimate the faults. The estimation results are shown in Fig. 10.

The verification result shows that, due to the equivalent output-error injection, the estimation error of the above four faults can converge to the zero domain in 2 seconds and maintains sliding motion, which indicates high sensitivity. In addition, due to the design of H_∞, the fault estimation results can be stabilized in the zero domain, without significant chattering, which suggests a high estimation accuracy.

The above analysis shows that the timeliness, fault identification capability, and fault separation capability of the joint sliding mode observers are far superior to the conventional method. During the fault estimation, the scheme, which is introduced in this paper, weakens the effect of chattering significantly, which is indicative of both high sensitivity and high estimation accuracy.

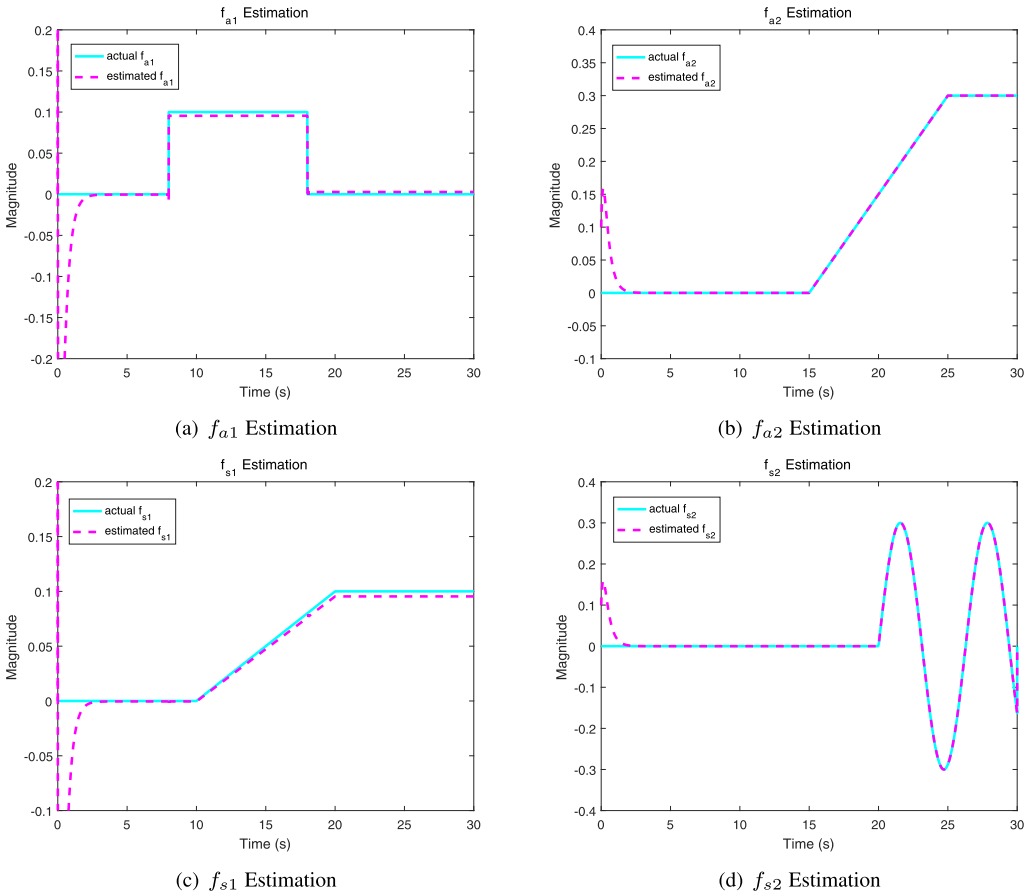

(a) f_{a1} Estimation (b) f_{a2} Estimation

(c) f_{s1} Estimation (d) f_{s2} Estimation

FIGURE 10. Estimation of multi-faults.

V. CONCLUSION

In this paper, we proposed a multi-fault diagnosis scheme of the aero-engine control system using joint sliding mode observers. Firstly, a mathematical multi-fault model was established to describe the actuator and sensor faults accurately and comprehensively. Then, we constructed the joint sliding mode observers, using the sliding mode variable structure term, to weaken coupling between the different faults. This enables the detection and isolation of each fault. After isolating the faults, we designed observers to estimate the fault characteristics. The design of H_∞ can suppress the impact of uncertain factors, and the equivalent output error injection term produces a more accurate fault estimation. Compared with the conventional method, the advantages of the new method are: When multi-faults occur in the control system, the proposed scheme can effectively diagnose actuator and sensor faults including jumping faults, gradual faults and sinusoidal faults. During establishing multi-fault model, sensor faults are translated into pseudo-actuator faults through integral transformation, i.e., sensor faults have the same form as actuator faults, which makes the description of multi-faults more accurate and comprehensive, and simplifies the fault diagnosis scheme design significantly. During the FDI process, the proposed scheme showed high sensitivity, fault identification capability, and separation capability, while weakening the coupling effect. During the fault estimation, the proposed pseudo-sliding form can reduce the chattering problem and the H_∞ design can suppress the impact of interference. The benefits of reducing the effect of chattering, higher sensitivity, and higher estimation accuracy are also noticeable.

A future research direction is to extend the method to different types of aero-engines, and to design observers for different system features, which would enhance the capability of the method. We verified the multi-fault diagnosis at the exact operating point, but the robustness at different fan rotor speeds in the full flight envelope remains to be studied. In addition, when designing the observers, the fault diagnosis scheme can be further improved by combining aero-engine component degradation and gas-path faults. This would enhance the comprehensiveness of the method. Hence, a more complete fault diagnosis scheme can be constructed, which improves both aero-engine safety and stability effectively, and extends the operating life of an aero-engine.

ACKNOWLEDGMENT

As a national key project, the National Science and Technology Major Project mainly carries out basic research on aero engine and gas turbine, with a view to improving the design level of aero engine and gas turbine. The Funds of the Central Universities aim to build kind of fundamental research of the intelligent aero-engine.

REFERENCES

[1] S. A. Gadsden, Y. Song, and S. R. Habibi, "Novel model-based estimators for the purposes of fault detection and diagnosis," *IEEE/ASME Trans. Mechatronics*, vol. 18, no. 4, pp. 1237–1249, Aug. 2013.

[2] R. Martinez-Guerra and J. L. Mata-Machuca, *Fault Detection and Diagnosis in Nonlinear Systems: A Differential and Algebraic Viewpoint*. Berlin, Germany: Springer, 2014.

[3] S. X. Ding, *Model-Based Fault Diagnosis Techniques*. Berlin, Germany: Springer, 2013.

[4] W. Chen, W.-T. Chen, M. Saif, M.-F. Li, and H. Wu, "Simultaneous fault isolation and estimation of lithium-ion batteries via synthesized design of Luenberger and learning observers," *IEEE Trans. Control Syst. Technol.*, vol. 22, no. 1, pp. 290–298, Jan. 2014.

[5] G. Chang, "Kalman filter with both adaptivity and robustness," *J. Process Control*, vol. 24, no. 3, pp. 81–87, Mar. 2014.

[6] J. Y. Lau, W. Liang, H. C. Liaw, and K. K. Tan, "Sliding mode disturbance observer-based motion control for a piezoelectric actuator-based surgical device: Sliding mode disturbance observer-based motion control," *Asian J. Control*, vol. 20, no. 3, pp. 1194–1203, May 2018.

[7] D. Zhao, S. K. Spurgeon, and X. Yan, "An adaptive finite time sliding mode observer," in *New Perspectives and Applications of Modern Control Theory*. New York, NY, USA: Institute of Electrical and Electronics Engineers, 2018.

[8] T. Kim, H. Shim, and D. D. Cho, "Distributed Luenberger observer design," in *Proc. IEEE 55th Conf. Decision Control (CDC)*, Dec. 2016.

[9] X. T. Tong, A. J. Majda, and D. Kelly, "Nonlinear stability of the ensemble Kalman filter with adaptive covariance inflation," *Commun. Math. Sci.*, vol. 14, no. 5, pp. 1283–1313, 2016.

[10] S. E. Li, G. Li, J. Yu, C. Liu, B. Cheng, J. Wang, and K. Li, "Kalman filter-based tracking of moving objects using linear ultrasonic sensor array for road vehicles," *Mech. Syst. Signal Process.*, vol. 98, pp. 173–189, Jan. 2018.

[11] Y. Wang, H. Fang, L. Zhou, and T. Wada, "Revisiting the state-of-charge estimation for lithium-ion batteries: A methodical investigation of the extended Kalman filter approach," *IEEE Control Syst.*, vol. 37, no. 4, pp. 73–96, Aug. 2017.

[12] K. P. B. Chandra and D.-W. Gu, "Cubature Kalman filter: Methods and applications," in *Nonlinear Filtering*. Cham, Switzerland: Springer, 2019.

[13] Z. Deng, D. Chu, F. Tian, Y. He, C. Wu, Z. Hu, and X. Pei, "Online estimation for vehicle center of gravity height based on unscented Kalman filter," in *Proc. 4th Int. Conf. Transp. Inf. Saf. (ICTIS)*, Aug. 2017.

[14] F. Li, L. Wu, P. Shi, and C.-C. Lim, "State estimation and sliding mode control for semi-Markovian jump systems with mismatched uncertainties," *Automatica*, vol. 51, pp. 385–393, Jan. 2015.

[15] V. Utkin, "Discussion aspects of high-order sliding mode control," *IEEE Trans. Autom. Control.*, vol. 61, no. 3, pp. 829–833, Mar. 2016.

[16] B. Sheng, F. Yong, and L. Sun, "Robust sliding mode observer design of nonlinear uncertain systems," *J. Harbin Inst. Technol.*, vol. 36, no. 5, pp. 613–616, 2004.

[17] Y. Al Younes, H. Noura, M. Muflehi, A. Rabhi, and A. El Hajjaji, "Model-free observer for state estimation applied to a quadrotor," in *Proc. Int. Conf. Unmanned Aircr. Syst. (ICUAS)*, Jun. 2015.

[18] B. Li, Q. Hu, Y. Yang, and O. A. Postolache, "Finite-time disturbance observer based integral sliding mode control for attitude stabilisation under actuator failure," *IET Control Theory Appl.*, vol. 13, no. 1, pp. 50–58, Jan. 2019.

[19] Z. Zhou, Z. Gao, Y. Xu, J. Lin, and T. Cao, "Fault tolerant attitude control design for rigid satellite using sliding mode observer technique," in *Proc. IEEE Chin. Guid., Navigat. Control Conf. (CGNCC)*, Aug. 2016.

[20] J. Fei and C. Lu, "Adaptive sliding mode control of dynamic systems using double loop recurrent neural network structure," *IEEE Trans. Neural Netw. Learn. Syst.*, vol. 29, no. 4, pp. 1275–1286, Apr. 2018.

[21] M. Chen, S.-D. Chen, and Q.-X. Wu, "Sliding mode disturbance observer-based adaptive control for uncertain MIMO nonlinear systems with deadzone," *Int. J. Adapt. Control Signal Process.*, vol. 31, no. 7, pp. 1003–1018, Jul. 2017.

[22] L. Yu, J. Huang, and S. Fei, "Sliding mode switching control of manipulators based on disturbance observer," *Circuits Syst. Signal Process.*, vol. 36, no. 6, pp. 2574–2585, Jun. 2017.

[23] S. Moussaoui and A. Boulkroune, "Stable adaptive fuzzy sliding-mode controller for a class of underactuated dynamic systems," in *Recent Advances in Electrical Engineering and Control Applications*. Cham, Switzerland: Springer, 2017.

[24] J. Mao, L. Wang, C. Gao, and S. Yang, "Research on inductive non-contact online cable fault diagnosis method," *Chin. J. Sci. Instrum.*, vol. 38, no. 7, pp. 1579–1588, 2017.

[25] J. Lu, D. Chen, J. Wang, and W. Li, "An investigation of model-based design framework for aero-engine control systems," in *Proc. Chin. Intell. Syst. Conf.*, 2016, pp. 625–638.

[26] J. Zhang, M. A. Wenpeng, L. I. Linjie, and Y. Liu, "Design and implementation of aeroengine fault diagnosis system," *Comput. Eng. Appl.*, vol. 50, no. 16, pp. 232–236, Aug. 2014.

[27] S. X. Ding, *Model-Based Fault Diagnosis Techniques: Design Schemes, Algorithms and Tools*, vol. 49, no. 15. Berlin, Germany: Springer, 2016, pp. 50–56.

[28] R. C. Avram, "A unified nonlinear adaptive approach for the fault diagnosis of aircraft engines," Wright State Univ., Dayton, OH, USA, Tech. Rep. wright1332784433, 2012.

[29] F. Lu and J. Huang, "Fault diagnosis for aero-engine based on ESVR information fusion," *J. Basic Sci. Eng.*, vol. 18, no. 6, pp. 982–989, 2010.

[30] N. Meskin, M. El-Koukoj, M. Benammar, R. Langari, and M. Al-Naemi, "Multiple sensor fault diagnosis for non-linear and dynamic system by evolving approach," *Inf. Sci.*, vol. 259, no. 1, pp. 346–358, 2014.

[31] F. Zhu, B. Li, L. Zhao, and Z. Yun, "Sensor fault diagnosis and classification in aero-engine," in *Proc. 1st Symp. Aviation Maintenance Manage.*, 2014, pp. 397–411.

[32] Y. Zhang, "Actuator fault-tolerant control for discrete systems with strong uncertainties," *Comput. Chem. Eng.*, vol. 33, no. 11, pp. 1870–1878, Nov. 2009.

[33] S. Borguet and O. Léonard, "A sensor-fault-tolerant diagnosis tool based on a quadratic programming approach," *J. Eng. Gas Turbines Power*, vol. 130, no. 2, 2008, Art. no. 021605.

[34] T.-M. Yoon, J.-S. Lee, and K.-B. Lee, "Rotor position estimation method of IPMSM using HF signal injection and sliding-mode controller," *IEEJ Trans. Elect. Electron. Eng.*, vol. 9, no. S1, pp. S56–S63, Oct. 2014.

[35] Y. Dong, P. Yang, W. Ma, and B. Ma, "Sliding mode robust adaptive fault-tolerant control design for uncertain time-delay systems," in *Proc. IEEE Chin. Guid., Navigat. Control Conf. (CGNCC)*, Aug. 2016.

[36] R. J. Patton and J. Chen, "On eigenstructure assignment for robust fault diagnosis," *Int. J. Robust Nonlinear Control*, vol. 10, no. 14, pp. 1193–1208, Dec. 2000.

[37] R. Behinfaraz, M. Badamchizadeh, and A. R. Ghiasi, "An adaptive method to parameter identification and synchronization of fractional-order chaotic systems with parameter uncertainty," *Appl. Math. Model.*, vol. 40, nos. 7–8, pp. 4468–4479, Apr. 2016.

[38] Y. Han, Y. Kao, and C. Gao, "Robust sliding mode control for uncertain discrete singular systems with time-varying delays and external disturbances," *Automatica*, vol. 75, pp. 210–216, Jan. 2017.

[39] A. Sofyalı, E. M. Jafarov, and R. Wisniewski, "Robust and global attitude stabilization of magnetically actuated spacecraft through sliding mode," *Aerosp. Sci. Technol.*, vol. 76, pp. 91–104, May 2018.

[40] Y. Li, "Optimal guaranteed cost control of linear uncertain system: An LMI approach," *Kongzhi Lilun Yu Yinyong/Control Theory Appl.*, vol. 17, no. 3, pp. 423–428, 2000.

[41] P. Lesniewski, "Sliding mode control with time-varying sliding hyperplanes: A survey," in *Proc. 18th Int. Carpathian Control Conf. (ICCC)*, May 2017.

[42] J. Ma, S. Ni, W. Xie, and W. Dong, "Discrete time integral sliding-mode control for systems with matched and unmatched uncertainties," in *Proc. IEEE Int. Conf. Inf. Autom.*, Aug. 2015, pp. 2930–2936.

[43] L. Mengmeng, Q. Dehui, L. Yuan, and W. Qinglin, "Adaptive sliding mode control with linear matrix inequality based on a DEAP flexible actuator," in *Proc. 29th Chin. Control Decision Conf. (CCDC)*, May 2017.

LINFENG GOU received the Ph.D. degree from Northwestern Polytechnical University, in 2010. He is currently an Associate Professor of power control engineering and the Vice President with the Power and Energy College, Northwestern Polytechnical University. He has participated in many national key projects. His main research interests include fault diagnosis and fault tolerant control of aero-engine control systems.

YAWEN SHEN received the B.S. degree from the School of Power and Energy, Northwestern Polytechnical University, Xi'an, China, where she is currently pursuing the master's degree with the School of Power and Energy. Her research interests include aero-engine fault diagnosis and health management.

HUA ZHENG received the Ph.D. degree from Northwestern Polytechnical University, in 2011. He is currently an Associate Professor of power control engineering. His main research interests include signal processing, modern measurement and control technology.

XIANYI ZENG received the B.S. degree in aircraft engineering from the Zhengzhou University of Aeronautics, Zhengzhou, China, in 2018. She is currently pursuing the master's degree with the School of Power and Energy, Northwestern Polytechnical University, Xi'an, China. Her research interests include aero engine modeling and analysis based on the industrial Internet of Things.